

# Photolytically generated aerosols in the mesosphere and thermosphere of Titan

Mao-Chang Liang<sup>1,2</sup>, Yuk L. Yung<sup>2</sup>, and Donald E. Shemansky<sup>3</sup>

## ABSTRACT

Analysis of the Cassini Ultraviolet Imaging Spectrometer (UVIS) stellar and solar occultations at Titan to date include 12 species: N<sub>2</sub> (nitrogen), CH<sub>4</sub> (methane), C<sub>2</sub>H<sub>2</sub> (acetylene), C<sub>2</sub>H<sub>4</sub> (ethylene), C<sub>2</sub>H<sub>6</sub> (ethane), C<sub>4</sub>H<sub>2</sub> (diacetylene), C<sub>6</sub>H<sub>6</sub> (benzene), C<sub>6</sub>N<sub>2</sub> (dicyanodiacetylene), C<sub>2</sub>N<sub>2</sub> (cyanogen), HCN (hydrogen cyanide), HC<sub>3</sub>N (cyanoacetylene), and aerosols distinguished by a structureless continuum extinction (absorption plus scattering) of photons in the EUV. The introduction of aerosol particles, retaining the same refractive index properties as tholin with radius  $\sim 125$  Å and using Mie theory, provides a satisfactory fit to the spectra. The derived vertical profile of aerosol density shows distinct structure, implying a reactive generation process reaching altitudes more than 1000 km above the surface. A photochemical model presented here provides a reference basis for examining the chemical and physical processes leading to the distinctive atmospheric opacity at Titan. We find that dicyanodiacetylene is condensable at  $\sim 650$  km, where the atmospheric temperature minimum is located. This species is the simplest molecule identified to be condensable. Observations are needed to confirm the existence and production rates of dicyanodiacetylene.

*Subject headings:* planetary systems—radiative transfer—atmospheric effects—planets and satellites: individual (Titan)—methods: data analysis, numerical

## 1. Introduction

Titan is Nature's laboratory for organic synthesis. The major molecules in the atmosphere are N<sub>2</sub> and CH<sub>4</sub>. The coupled chemistry between nitrogen and carbon leads to high

---

<sup>1</sup>Research Center for Environmental Changes, Academia Sinica, Taipei 115, Taiwan

<sup>2</sup>Division of Geological and Planetary Sciences, California Institute of Technology, Pasadena, CA 91125, USA

<sup>3</sup>Planetary and Space Science Division, Space Environment Technologies, Pasadena, CA 91107, USA

abundances of nitrogen/carbon compounds, such as hydrogen cyanide (see, e.g., Yung et al. 1984; Coustenis et al. 2003; Wilson & Atreya 2004). This is caused primarily by the low gravity of Titan which allows hydrogen to escape readily (e.g., Yelle et al. 2006), resulting in low hydrogen abundance and rich hydrocarbon production. When the order of hydrocarbons and nitriles is large enough, they condense to form aerosols and precipitate. The stratosphere is a major region for the production of haze (e.g., McKay et al. 2001). The estimated vertically integrated rate is  $0.5\text{-}2 \times 10^{-14}$  g cm<sup>-2</sup> s<sup>-1</sup> with haze formation taking place in the 300 km to 500 km region. Total mass loading according to McKay et al. (2001) was about 250 mg m<sup>-2</sup>, made by molecules with a C/N ratio of 2-4 and a C/H ratio of about unity. The present work obtains about 100 mg m<sup>-2</sup> (assuming density 3 g cm<sup>-3</sup>) above 300 km.

## 2. Cassini UVIS Observations

On 13 December 2004, the Cassini UVIS recorded the occultation of two stars,  $\lambda$  Sco (Shaula; latitude  $-36^\circ$ ) and  $\alpha$  Vir (Spica; latitude range of  $+63^\circ$  and  $+48^\circ$ ), near the end of the second Titan flyby ( $T_B$ ) (details are referred to Shemansky et al. 2005; Shemansky 2006; Shemansky et al. 2007). The fully reduced results from  $\lambda$  Sco only are referenced here. The vertical distribution of the aerosol component as the terminal product of N<sub>2</sub>/CH<sub>4</sub> physical and chemical processes, is of primary interest to this Letter. The spectral region 1850-1900 Å (SP1) is effectively free of the measurable hydrocarbon and cyano species in this atmosphere apart from aerosols, and this region is used photometrically to trace the aerosol structure. The vertical profile of extinction for SP1 below 1000 km was carried out at the highest possible ray-height resolution (3-5 km) in order to reveal possible structure in the distribution.

The best fit to the transmission spectrum at impact parameter  $h = 514$  km is shown in Figure 1 as an example of spectral reduction. Table 1 shows the extracted line-of-sight abundances from this element of the occultation. Figure 2 shows the aerosol density vertical distribution (heavy dots) derived from the reduction of the  $\lambda$  Sco occultation, compared to the derived CH<sub>4</sub> profile (dashed line). The reduced data extend from  $h = 330$  km to 970 km where signal noise terminates the reduction (see Shemansky et al. 2007 for details). The remarkable property of the aerosol distribution is the sudden departure from tracking the CH<sub>4</sub> abundance at  $h = 468$  km toward higher altitudes. The interval between 468 km and 550 km where abundance remains approximately constant, is interpreted as a primary aerosol source region. The density extraction is a direct deconvolution of the abundance distribution. The derivation is based on assumed spherical uniformity and assumed uniformity in composition

with altitude. The observations show measurable simple scattering in the 1800 Å region at  $h = 1250$  km, indicating that aerosols are extensively distributed into the thermosphere.

The cross sections for extinction of UV light by aerosols were computed using the complex refractive index measured by Khare et al. (1984) for solid state tholins, and the scattering code of Mishchenko & Travis (1998). Representative complex indices of refraction at 588, 1215, 1631 and 2384 Å are (0.963, 0.62), (1.74, 0.37), (1.65, 0.24) and (1.68, 0.21), respectively. Assuming a mean radius of 125 Å for aerosols, the corresponding extinction cross sections are  $2.4 \times 10^{-12}$ ,  $3.9 \times 10^{-13}$ ,  $2.0 \times 10^{-13}$  and  $1.2 \times 10^{-13}$  cm<sup>2</sup>, respectively. The actual computation used in this work has a finer wavelength grid. Note that the current UVIS data set no constraint on the vertical variation of the optical property of aerosols.

Extinction of the EUV stellar photons is dominated by CH<sub>4</sub> in the 1100 Å to 1400 Å region. At longer wavelengths the structure is a combination of the higher order hydrocarbon and cyano species. The C<sub>6</sub>H<sub>6</sub> cross section peaks at 1759.9-1815.1 Å, blended primarily with C<sub>2</sub>H<sub>4</sub>. Dicyanodiacetylene has a cross section peak in the SP1 spectral region. Dicyanodiacetylene and benzene have not been detected in the absorption spectra (Shemansky et al. 2007). Aerosol extinction is detectable at ~970 km in the transmission spectra and dominates all absorbers at all wavelengths in the UVIS except for CH<sub>4</sub>, at altitudes below 400-450 km.

Figure 1 shows the contribution of aerosol extinction to the total measured optical depth at 514 km. In the spectral region SP1 aerosol extinction is entirely responsible for the optical depth. The measurable spectral region for extracting the aerosol component is 1500-1900 Å, where the wavelength dependence of extinction shows a proportionality to  $\lambda^{-1.5}$ . The Voyager and Cassini photometric observations in the UV spectral region (Porco et al. 2005; West et al. 2006) have revealed the presence of detached haze layers at Titan. The Cassini results show the presence of a latitudinally uniform detached layer near 500 km in forward scattered 3380 Å photons. The relationship of this phenomenon to the aerosols identified here requires further investigation. A comparison to Voyager results (Smith et al. 1982) shows that the major differences are that the apparent strong extinction by aerosols takes effect about 100 km higher for Voyager and significantly more extinction is evident for Voyager in the 700-1000 km region. The Voyager data show a broad extinction maximum near 770 km.

### 3. Photochemical Modeling

Vertical profiles of the major species have been calculated using a photochemical model. The photochemical reactions are taken from Yung et al. (1984), Yung (1987), and Moses et al.

(2000). The chemical scheme to  $C_6N_2$  is hypothesized to be similar to that to  $C_4N_2$ , as derived by Yung (1987) and summarized in Table 2. The temperature profile is based on the Cassini measurements (Figure 2, dotted line). The vertical eddy mixing profile is taken from Yung et al. (1984). The model simulation is diurnally averaged at low latitude. The incident UV flux is the mean between solar maximum and minimum. Table 1 provides a summary of model results. Sensitivity to the selection of hydrocarbon kinetics and that of kinetics and vertical eddy coefficients are shown by models D and WA04, respectively.

We fix the  $N_2$  abundance to that derived from the Cassini measurements. The model starts with a hydrostatic atmosphere. With the prescribed vertical diffusion coefficients and taking the photolysis of  $CH_4$  into account, the abundance of  $CH_4$  is overestimated (see Table 1), compared with the measurements. To bring the model into better agreement with the observations, we introduce an *ad hoc* advection which transports species other than  $N_2$  downward. The wind is prescribed with strength proportional to the inverse of the square root of atmospheric density. The wind speed reaches  $-20 \text{ cm s}^{-1}$  at the top of the model atmosphere ( $\sim 1500 \text{ km}$ ). The assumed downward wind is qualitatively consistent with global circulation that has a downward transport at mid to high latitudes (e.g., Lebonnois et al. 2001). A comparison with modeled  $CH_4$  abundances between models A and C is shown in Figure 3. We note that dynamics plays an important role in distributing photochemical products (e.g., Lebonnois et al. 2001), especially in the regions above  $\sim 500 \text{ km}$  (the regions of interest to this work) where the transport time is, in general, shorter than the chemical removal time of hydrocarbon and cyano species (e.g., Wilson & Atreya 2004); current simulations coupled with dynamics and photochemistry are limited to the regions below  $\sim 400 \text{ km}$  (Lebonnois et al. 2001). The latitudinal variations of hydrocarbon and cyano abundances (e.g., Flasar et al. 2005) are the consequence of atmospheric transport and photochemical processes.

The modeled profiles of HCN,  $HC_3N$ ,  $C_6H_6$ , and  $C_6N_2$  are presented in Figure 3. Calculated abundances are compared to extraction from observation at 514 km in Table 1. Comparisons between models and observations at other impact parameters will be deferred to a later paper. The results for five variations on the model at this impact parameter are given in Table 1. In general, our base models (models A and B) overestimate the abundances of hydrocarbons by as much as 10 times. An indication of the difference in the predicted model C and observed optical depth spectra is shown in Figure 1. Model C (Table 1) is too high relative to measured abundance in  $C_2H_6$  and  $C_4H_2$ . The modeled  $C_6N_2$ ,  $C_6H_6$ , and  $HC_3N$  are also well above the upper limits set by observation. There are two ways of reducing the abundances. (1) Faster transport of photochemical products to the lower atmosphere as in the model of Wilson & Atreya (2004) (model WA04). Comparing the transport time constant with the chemical destruction time, the abundances of  $C_2H_2$ ,  $C_2H_6$ , HCN, and  $C_2N_2$

have sensitivity to transport and those of  $C_2H_4$ ,  $C_4H_2$ ,  $C_6N_2$ ,  $C_6H_6$ , and  $HC_3N$  at  $\sim 500$  km are close to being in photochemical equilibrium (e.g., Wilson & Atreya 2004). (2) Relatively rapid two-body physicochemical processes forming aerosols as simulated in models C and D. The loss rates in these models are assumed to be proportional to the physical collision rates between aerosols (with radius  $125 \text{ \AA}$ ) and molecules; adsorption reactions are assumed for all photochemical species listed in Table 1. The aerosol density is from Figure 2. The adsorption efficiency for this absolute loss, an assumed value of 0.01, yields the concentrations shown in Table 1. As described below, this process is required for explaining the aerosol abundance shown in Figure 2.

#### 4. Discussion

The source of aerosols has long been a puzzle in the atmosphere of Titan. It is generally believed that the synthesis of increasingly complex hydrocarbon and nitrogen compounds will eventually lead to saturation, resulting in coagulation and precipitation. However, the chemical composition of the condensible species has not yet been established. In this Letter, we propose that the simplest condensible compound is  $C_6N_2$ . The abundances of the higher order species in the UVIS observations are significantly lower than the present model calculations. Assuming that the model conversion rates for the  $CH_4$  source are basically correct, there is an implied loss rate for these species that is substantially higher than the model provides. The model calculation contains an absolute loss to the measured aerosols using a conservatively small adsorption probability. If a significant fraction of the implied loss is delivered to the production of aerosols, the model can be adjusted by assuming a larger irreversible adsorption probability and a consequent higher precipitation rate for the aerosols. This will bring the model abundances into better conformance with observation, but will not necessarily resolve differences in partitioning, and may not resolve issues raised in regard to rate limits for the mass flow process that cycles to the surface. We propose that the aerosol formation is initiated by the condensation of  $C_6N_2$  and adsorption to external meteoritic dust; both serve seeds for aerosol formation. The subsequent physical processes of adsorption on the existing aerosols and (photo)chemistry converting these clusters into refractory tholins constitute the production and maintenance of the aerosol distribution. Hunten (2006) has recently proposed that haze is a major sink of ethane at Titan. The process of formation of aerosols requires the stable adsorption of the higher order hydrocarbon and nitrile species.

The production rate of  $C_6N_2$  in the model limits the production rate of aerosols from this direct path. The saturation density of dicyanodiacetylene shown in Figure 3 shows

that condensation can take place between  $\sim 550$  and  $800$  km. The volume production rate of  $C_6N_2$  in this region is quite uniform ( $\sim 1$  molecules  $cm^{-3} s^{-1}$ ); the column integrated ( $550$ - $800$  km) rate is  $\sim 10^7$  molecules  $cm^{-2} s^{-1}$ , or  $\sim 2 \times 10^{-15}$  g  $cm^{-2} s^{-1}$ . This contribution is a small fraction of the total aerosol production, but is extremely important as a source of condensation nuclei. The maximum rate of aerosol production, however, is set by the total photolysis rate of  $CH_4$  which is on the order of  $10^{10}$  molecules  $cm^{-2} s^{-1}$ , or  $2 \times 10^{-13}$  g  $cm^{-2} s^{-1}$  of carbon, a result that is independently corroborated by the  $H_2$  escape flux (Yelle et al. 2006). The rate of removal of molecules by the existing particles in model C is close to this maximum rate. However, the resulting aerosol profile (thin solid line in Figure 2) underestimates the observed aerosol abundances above  $\sim 800$  km, suggesting an additional source at the top of the atmosphere, equivalent to a downward flux of  $5 \times 10^{-14}$  g  $cm^{-2} s^{-1}$  (thick solid line). This flux is consistent with that inferred from the Cassini Ion Neutral Mass Spectrometer measurements (Waite et al. 2007) on the basis of ion chemistry not considered here. Note that a sedimentation velocity of  $0.25$   $cm s^{-1}$  has to be imposed in order to match the observed aerosol profile; this implies that the radius of the aerosols must be  $\sim 125$  Å in the mesosphere and thermosphere.

We emphasize that there are significant uncertainties in rate process quantities and stronger constraints are needed. Laboratory measurements for the adsorption rates on aerosols in collision with the high order molecules are required to verify this process, and to provide a better constraint to the aerosol mass loading in the atmosphere of Titan. In addition, the photochemical paths to high order hydrocarbon and nitrile compounds such as  $C_6N_2$  and  $C_6H_6$  are speculative. Atmospheric dynamics in the mesosphere of Titan also plays a central role in molecule/aerosol mixing. Further laboratory measurements and Cassini observations will provide valuable information in refining our understanding of the chemical, dynamical, and microphysical processes in the atmosphere of Titan.

This research was supported by NASA grant NNG06GF33G and Cassini grant JPL.1256000 to the California Institute of Technology. DES acknowledged support by NASA grant NNG06GH76G and Cassini UVIS Program contract 1531660 to Space Environment Technologies.

## REFERENCES

- Cabane, M, E. Chassefiere, & G. Israel 1992. *Icarus* 96, 176
- Coustenis, A., A. Salama, B. Schulz, S. Ott, E. Lellouch, T. Encrenaz, D. Gautier, & H. Feuchtgruber 2003. *Icarus* 161, 383

- Flasar, F. M., & colleagues 2005. *Science* 308, 975  
Gautier, T. Owen, H. E. Matthews, & G. Paubert 1997. *Icarus* 126, 170
- Hunten, D. M. 2006. *Nature* 443, 669
- Khare, B. N., C. Sagan, E. T. Arakawa, F. Suits, T. A. Callcott, & M. W. Williams 1984. *Icarus* 60, 127
- Lebonnois, S., D. Toublanc, F. Hourdin, & P. Rannou 2001. *Icarus* 152, 384
- McKay, C. P., A. Coustenis, R. E. Samuelson, M. T. Lemmon, R. D. Lorenz, M. Cabane, P. Rannou, & P. Drossart 2001. *Planet. Space Sci.* 49, 79.
- Mishchenko, M. I., & L. D. Travis 1998. *Journal of Quantitative Spectroscopy & Radiative Transfer* 60, 309.
- Moses, J. I., B. Bezard, E. Lellouch, G. R. Gladstone, H. Feuchtgruber, & M. Allen 2000. *Icarus* 143, 244.
- Moses, J. I., T. Fouchet, B. Bezard, G. R. Gladstone, E. Lellouch, & H. Feuchtgruber 2005. *J. Geophys. Res.* 110,
- Opansky, B. J., & S. R. Leone 1996. *Journal of Physical Chemistry* 100, 4888.
- Proco, C. C., et al. 2005. *Nature*, 434, 159
- Saggiomo, A. J. 1957. *Journal of Organic Chemistry* 22, 1171.
- Shemansky, D. E. 2006. COSPAR, C3.1, 88338533
- Shemansky, D. E., et al. 2007. In preparation
- Shemansky, D. E., A. I. F. Stewart, R. A. West, L. W. Esposito, J. T. Hallett, & X. M. Liu 2005. *Science* 308, 978
- Smith, G. R., D. F. Strobel, A. L. Broadfoot, B. R. Sandel, D. E. Shemansky, J. B. Holberg 1982. *J. Geophys. Res.* 87, 1351
- West, R. A., P. Dumont, D. Tice, B. Cassler, J. Snow, R. Cleaver, D. Shemansky, Y. Yung, K. Larsen, M. Evans, L. Esposito, C. Porco 2006. *BAAS*, 38, 22.02
- Waite, J. H., Jr., D. T. Young, T. E. Cravens, A. J. Coates, F. J. Crary, B. Magee, and J. Westlake 2007. *Science*, in press

Wilson, E. H., & S. K. Atreya 2004. *J. Geophys. Res.* 109, E06002,  
DOI:10.1029/2003JE002181

Yelle, R. V., N. Borggren, V. de la Haye, , W. T. Kasprzak , H. B. Niemann, I. Muller-  
Woodarg, & J. H. Waite Jr. 2006. *Icarus* 72, 468

Yung, Y. L. 1987. *Icarus* 72, 468

Yung, Y. L., M. Allen, & J. P. Pinto 1984. *ApJS* 55, 465

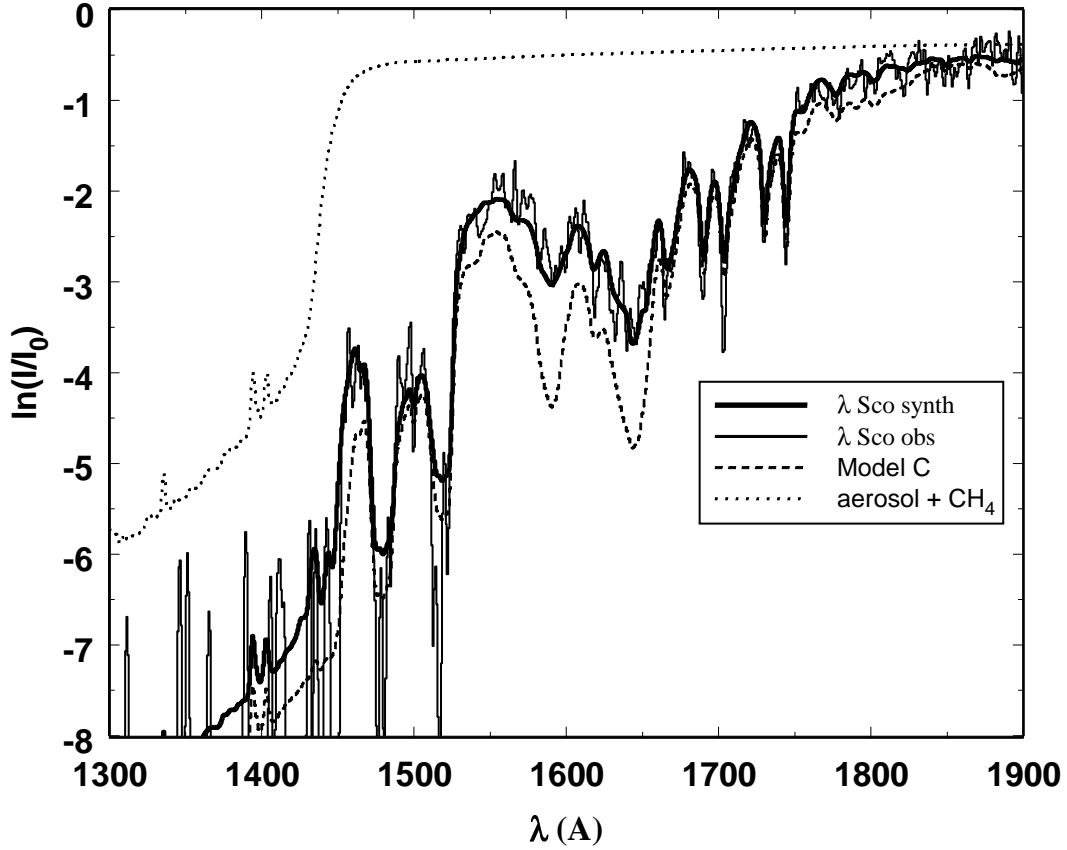


Fig. 1.— The transmission spectrum of the UVIS  $\lambda$  Sco occultation integrated over the impact parameter 514 km to 537 km (light line), compared to the best-fit synthesis (Shemansky et al. 2007) using the combined identified species (heavy line), and to model C from the present physical chemistry code (dashed line). The dotted line shows the aerosol component combined with the  $\text{CH}_4$  absorber in this reduction. The  $\text{CH}_4$  absorber ( $\lambda < 1490 \text{ \AA}$ ) is included with aerosol here as a means of including a large part of the impact of instrument point spread function on the fitting process. The optical depth in region SP1 is entirely attributed to aerosol extinction; The small difference between the observed data and the aerosol component at SP1 is an artifact of the UVIS EUV instrument point spread function. The abundances of the species for this case are given in Table 1. See text.

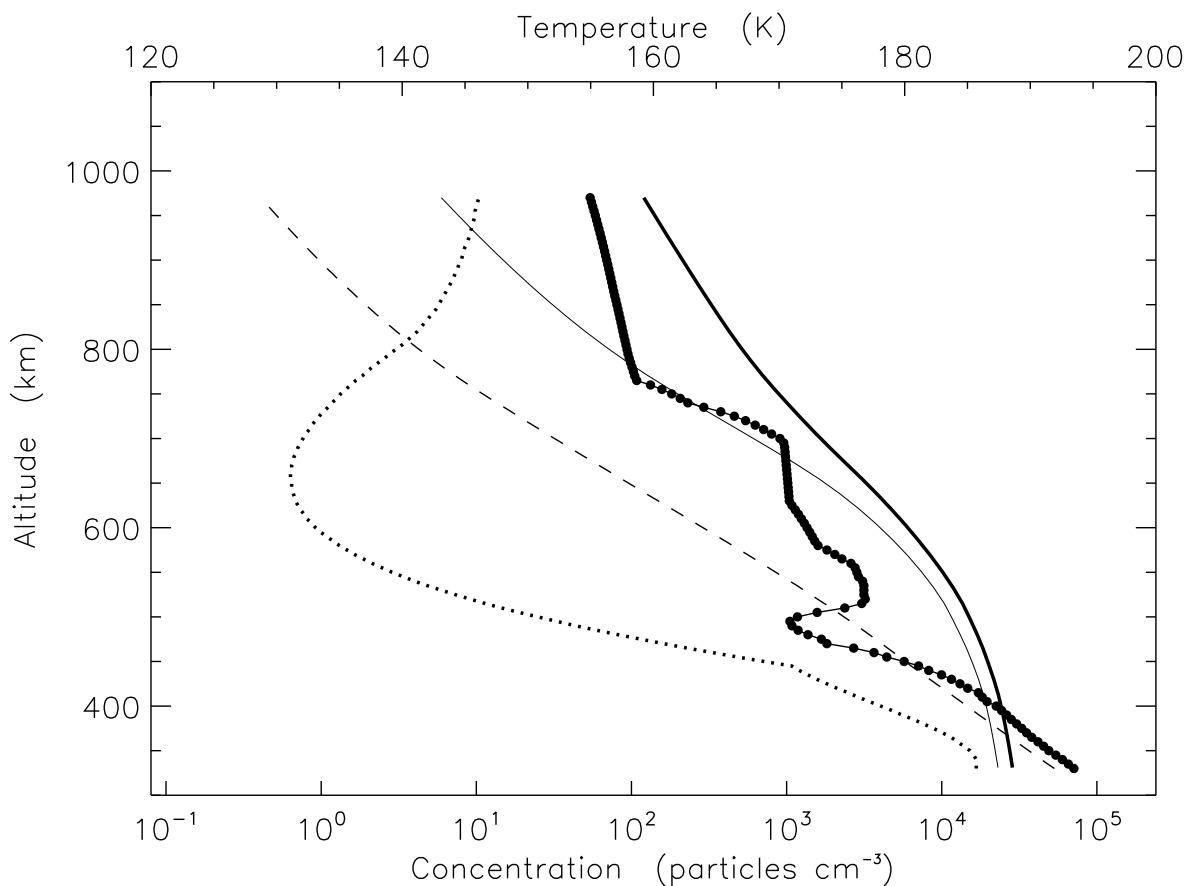


Fig. 2.— Aerosol density (heavy dots) derived from the UVIS  $\lambda$  Sco occultation compared to the CH<sub>4</sub> (dashed line) scaled by  $10^{-9}$  (Shemansky et al. 2005; Shemansky 2006). The increase of the mixing ratio of the UVIS aerosols through the mesosphere to at least 1000 km implies that the production of aerosols must take place at significant rates throughout the mesosphere and thermosphere. The UVIS derived temperature profile is shown by the dotted line, which reflects a correction to the one presented by Shemansky et al. (2005). The model aerosol profiles are shown by the thin and solid lines (see text). The over- and underestimations are due to the fact that we assume a constant sedimentation velocity of  $0.25 \text{ cm s}^{-1}$ , calculated at 535 km (Cabane et al. 1992).

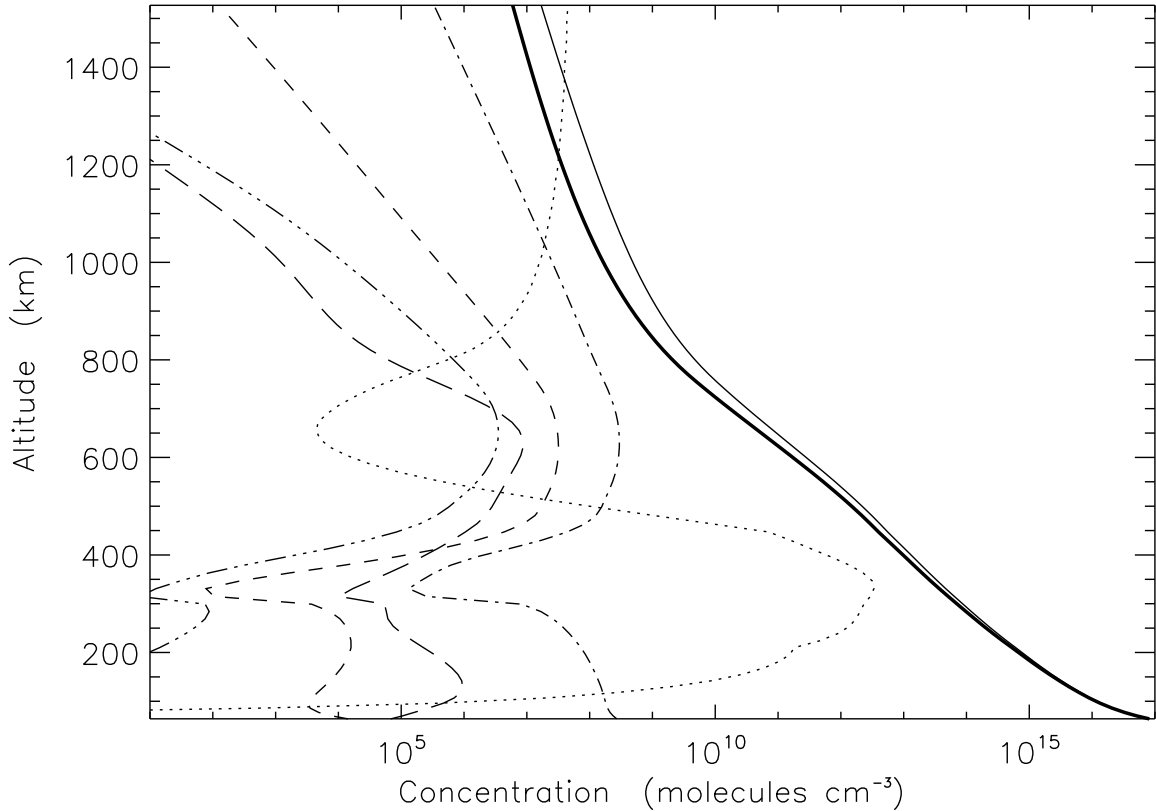


Fig. 3.— Modeled (model C) vertical profiles for CH<sub>4</sub> (thick solid), HC<sub>3</sub>N (dashed), HCN (dash-dotted), C<sub>6</sub>N<sub>2</sub> (triple-dot-dashed), and C<sub>6</sub>H<sub>6</sub> (long-dashed). Thin solid line represents modeled CH<sub>4</sub> by model A. The saturation density of C<sub>6</sub>N<sub>2</sub> extrapolated from high temperature measurements (295-369 K, Saggiomo 1957) is shown by dotted line. The resulting H<sub>2</sub> ( $3 \times 10^{-3}$ ) and CH<sub>4</sub> (2.3%) mixing ratios at 1174 km and H<sub>2</sub> escape flux ( $7 \times 10^9$  molecules cm<sup>-2</sup> s<sup>-1</sup>) at the top are in good agreement with the observations ( $4 \pm 1 \times 10^{-3}$ ,  $2.7 \pm 0.1\%$ , and  $1.2 \pm 0.2 \times 10^{10}$  molecules cm<sup>-2</sup> s<sup>-1</sup>, respectively) (Yelle et al. 2006).

Table 1. Summary of Model Results

Molecule	Cassini	Model A	Model B	Model C	Model D	WA04
$\text{N}_2$ ( $\times 10^{21}$ )	5.8	5.8	5.8	5.8	5.8	5.8
$\text{CH}_4$ ( $\times 10^{19}$ )	6.0	15	9.4	9.5	9.7	13
$\text{C}_2\text{H}_2$ ( $\times 10^{17}$ )	2.1	15	9.1	1.9	1.7	1.5
$\text{C}_2\text{H}_4$ ( $\times 10^{16}$ )	4.0	9.3	5.7	4.0	2.0	3.4
$\text{C}_2\text{H}_6$ ( $\times 10^{16}$ )	7.0	200	110	17	9.2	20
$\text{HCN}$ ( $\times 10^{17}$ )	1.0	5.6	3.7	0.69	0.53	0.017
$\text{C}_4\text{H}_2$ ( $\times 10^{15}$ )	4.5	59	37	12	2.1	41
$\text{C}_6\text{N}_2$ ( $\times 10^{14}$ )	<1.0	15	16	5.7	8.0	...
$\text{C}_6\text{H}_6$ ( $\times 10^{14}$ )	<1.4	18	13	12	0.041	0.21
$\text{HC}_3\text{N}$ ( $\times 10^{15}$ )	<3.9	27	25	6.9	7.8	0.96
$\text{C}_2\text{N}_2$ ( $\times 10^{15}$ )	<4.0	0.84	1.2	0.34	0.42	0.00035
Tholin ( $\times 10^{11}$ )	4.6	...	...	...	...	...

Note. — Values are line-of-sight column integrated abundances, in molecules  $\text{cm}^{-2}$ , reported by matching the observed  $\text{N}_2$  abundance. Model A: hydrostatic atmosphere. Model B: non-hydrostatic atmosphere, an *ad hoc* downward wind and extinction due to the derived tholins are assumed (see text). Model C: same as Model B but also with additional sinks for the tabulated nine photochemical species (see text). Model D: same as model C but with the updated hydrocarbon chemistry from Moses et al. (2005). WA04: model results from Wilson & Atreya (2004). Note that in this Letter, the microphysical processes of  $\text{C}_6\text{N}_2$  are not solved self-consistently; and hence, the tabulated abundances of  $\text{C}_6\text{N}_2$  do not reflect the removal by condensation.

Table 2. Chemical Reactions to C<sub>6</sub>N<sub>2</sub>

Label	Reactants	Products	Rate Coefficients <sup>a</sup>
R454	HC <sub>5</sub> N + hν	→ C <sub>4</sub> H + CN	= J(HC <sub>3</sub> N + hν → C <sub>2</sub> H + CN); (1)
R455	HC <sub>5</sub> N + hν	→ C <sub>5</sub> N + H	= J(HC <sub>3</sub> N + hν → C <sub>3</sub> N + H); (1)
R456	C <sub>6</sub> N <sub>2</sub> + hν	→ C <sub>5</sub> N + CN	= J(C <sub>4</sub> N <sub>2</sub> + hν → C <sub>3</sub> N + CN); (2)
R492	C <sub>3</sub> N + HC <sub>3</sub> N	→ C <sub>6</sub> N <sub>2</sub> + H	= k(C <sub>2</sub> H + C <sub>2</sub> H <sub>2</sub> → C <sub>4</sub> H <sub>2</sub> + H); (3)
R495	CN + C <sub>4</sub> H <sub>2</sub>	→ HC <sub>5</sub> N + H	= k(CN + C <sub>2</sub> H <sub>2</sub> → HC <sub>3</sub> N + H); (2)
R496	CN + HC <sub>5</sub> N	→ C <sub>6</sub> N <sub>2</sub> + H	= k(CN + HC <sub>3</sub> N → C <sub>4</sub> N <sub>2</sub> + H); (2)
R497	C <sub>5</sub> N + CH <sub>4</sub>	→ HC <sub>5</sub> N + CH <sub>3</sub>	= k(C <sub>3</sub> N + CH <sub>4</sub> → HC <sub>3</sub> N + CH <sub>3</sub> ); (2)
R498	C <sub>5</sub> N + C <sub>2</sub> H <sub>6</sub>	→ HC <sub>5</sub> N + C <sub>2</sub> H <sub>5</sub>	= k(C <sub>3</sub> N + C <sub>2</sub> H <sub>6</sub> → HC <sub>3</sub> N + C <sub>2</sub> H <sub>5</sub> ); (2)

<sup>a</sup>Estimated from the quoted reactions. Units are s<sup>-1</sup> for photolysis reactions (J) and cm<sup>3</sup> s<sup>-1</sup> for two-body reactions (k). The photolysis rate coefficients are given at the top of the model atmosphere. References: (1) Lebonnois et al. (2001) and Wilson & Atreya (2004); (2) Yung (1987); (2) Lebonnois et al. (2001) and Opansky & Leone (1996)